

High-quality proton bunch from laser interaction with a gas-filled cone target

H.Y.Wang,^{1,2} F.L.Zheng,² Y.R.Lu,¹ Z.Y.Guo,¹ X.T.He,² J.E.Chen,¹ and X. Q. Yan^{1,2,*}

¹*State Key Laboratory of Nuclear Physics and Technology,
Peking University, Beijing 100871, China*

²*Key Lab of High Energy Density Physics Simulation,
CAPT, Peking University, Beijing 100871, China*

(Dated: April 7, 2022)

Abstract

Generation of high-energy proton bunch from interaction of an intense short circularly polarized(CP) laser pulse with a gas-filled cone target(GCT) is investigated using two-dimensional particle-in-cell simulation. The GCT target consists of a hollow cone filled with near-critical gas-plasma and a thin foil attached to the tip of the cone. It is observed that as the laser pulse propagates in the gas-plasma, the nonlinear focusing will result in an enhancement of the laser pulse intensity. It is shown that a large number of energetic electrons are generated from the gas-plasma and accelerated by the self-focused laser pulse. The energetic electrons then transports through the foil, forming a backside sheath field which is stronger than that produced by a simple planar target. A quasi-monoenergetic proton beam with maximum energy of 181 MeV is produced from this GCT target irradiated by a CP laser pulse at an intensity of $2.6 \times 10^{20} W/cm^2$, which is nearly three times higher compared to simple planar target(67MeV).

PACS numbers: 52.38.Kd, 41.75.Jv, 52.35.Mw, 52.59.-f

*x.yan@pku.edu.cn

I. INTRODUCTION

With the rapid development of the chirped pulse amplification technique, generation of energetic ion beam by interactions of an ultra intense laser pulse with a solid target has become realizable. Such energetic ions can be promising for many scientific or societal applications, such as proton radiography[1], fast ignition for inertial confined fusion[2–4], or hadron-therapy[5]. For most of these applications, ion beams with high energy, low energy spread and high collimation are required.

Depending on the target parameters and laser intensity, ions can be accelerated by several different mechanisms, such as shock acceleration[6, 7], light-pressure acceleration[8, 10–12], Coulomb explosion[13], target-normal sheath acceleration (TNSA)[14–16], etc., as well as their combinations. In TNSA, the energetic electrons produced at the front of a target by the laser ponderomotive force propagate through the target into the backside vacuum can generate a sheath electrostatic field. The sheath field, of order 10^{12}V/m , can accelerate the ions on the target back surface to high energies. However, the proton beams obtained in this way are typically characterized by low particle density, large divergence, and almost 100% energy spread. An improved TNSA scheme, using a microstructured double-layer (DL) target, can decrease the energy spread. The possibility to generate 1.3 MeV proton beams with energy dispersion $\sim 25\%$ and 3 MeV carbon beams with energy dispersion $\sim 17\%$ using a microstructured DL target has already been demonstrated experimentally by Schwoerer et al.[17] and Hegelich et al.[18], respectively.

A tiny hollow metal cone was first introduced in fast ignition experiments to shield the igniting laser pulse from the underdense region of the precompressed fuel plasma[19], and a remarkable increase in the thermal fusion-neutron yield was observed. Since then the cone target was intensively examined both in experiments and simulations[20–32]. PIC simulations showed that a cone target could nonlinearly guide and focus a laser beam, and improve the efficiency of the coupling and transport of the energy into dense plasma[33, 34]. Accelerating proton beams using a cone target with open tip was also studied by Cao et al.[35], and energetic ion bunches of high density were observed. In this paper, we report that quasi-monoenergetic proton beam with peak energy of 130MeV and maximum energy of 181 MeV can be generated from a gas-filled cone target irradiated by a CP Gaussian laser pulse at an intensity of $2.6 \times 10^{20}\text{W/cm}^2$. The gas-filled cone target, as shown in Fig.1, consists

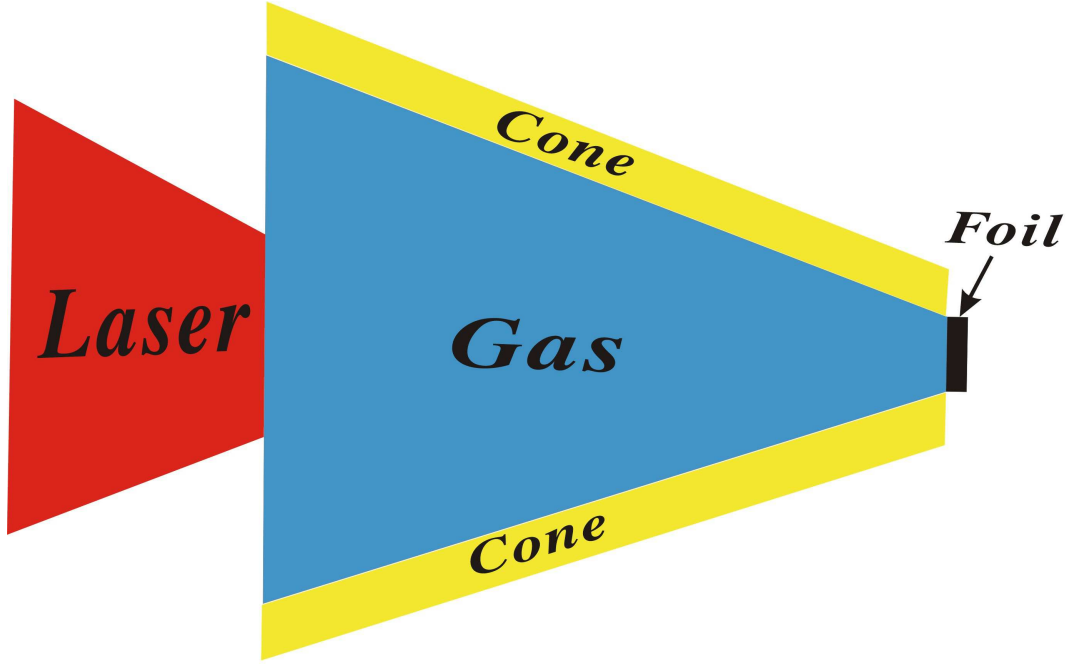


FIG. 1: (color online). Schematic view of the interaction of a laser pulse with a GCT target. The left trapezoid represents the laser pulse (red), the trapezoid irradiated by the laser pulse represents the gas-plasma (blue), the two parallelograms besides the gas-plasma represent the cone (orange), the rectangle on the tip of the cone represents the foil (dark).

of a hollow cone filled with near-critical heavy-ion gas-plasma and a thin foil attached to the tip of the cone. Our results indicate that, comparing with that from a simple proton target, energetic protons with smaller energy spread and higher energy can be obtained. This result can be attributed to the much higher electron density and temperature behind the foil and the small transverse size of the foil. The energetic electrons are generated from the gas-plasma and accelerated by the enhanced laser pulse, which undergoes self-focusing in gas-plasma and is even focused by the tip of the cone. These energetic electrons can easily propagate through the thin foil to form a stronger sheath field behind the foil (than that behind a planar target). Since the foil has a small transverse size, the protons in the foil are accelerated in the homogenous sheath field, so that the protons are accelerated longitudinally forward with smaller energy spread. In contrary to TNSA acceleration, here energetic electrons originate mainly from the gas rather than the solid target.

II. SIMULATION PARAMETERS

We carried out simulation using a fully relativistic particle-in-cell code (KLAP2D) [8, 9]. In simulations, the simulation box is $80\lambda \times 20\lambda$, where $\lambda = 1\mu m$ is the laser wavelength, and contains 3200×800 cells. A CP laser pulse with a peak laser intensity of $I_L = 2.6 \times 10^{20} W/cm^2$ is normally incident from the left side, The pulse has a Gaussian radial profile with $2\sigma = 10\lambda$ full width at half maximum and a trapezoidal shape longitudinally with $40T$ flat top and $1T$ ramps on both sides, where T is the laser period. The corresponding peak dimensionless laser amplitude $a_0 = eE/(m_e\omega c)$ is 9.8, where E , ω , c , m_e , and e are the laser electric field, frequency, speed of light in the vacuum, electron mass, and charge, respectively. The GCT target, as shown in Fig.1, consists of electrons, protons, and heavy carbon ions. The initial temperature of electrons, protons, and carbon ions is 10 eV. The cone has a width of $1\mu m$, and is located in $10 < z[\mu m] < 45$ with the diameters of the left and right cone openings of $16\mu m$ and $2\mu m$, respectively. For simplicity, the cone consists of carbon plasma with an electron density $n_e = 10n_c$, where $n_c = \pi m_e c^2 / (e\lambda)^2$ is the critical density. The carbon gas-plasma is full in the cone with density $n_e = 0.8n_c$. The foil with $2\mu m$ wide and $0.35\mu m$ thick is placed at $z = 45\mu m$. It consists of a proton-carbon mixed plasma with an electron density $n_e = 40n_c$, and the ratio of C:H=1:1.

III. SIMULATION RESULTS

A laser beam propagating in underdense plasma with a frequency ω_p smaller than the laser frequency ω undergoes relativistic self-focusing[36–40] as soon as its total power P exceeds the critical value

$$P_{cr} \approx 17(\omega/\omega_p)^2 GW; \quad (1)$$

The self-focusing is due to the relativistic mass increase of plasma electrons and the ponderomotive expulsion of electrons from the pulse region. Both effects lead to a local decrease of plasma frequency and an increase in refractive index. The strong non-linear self-focusing of the laser pulse propagating in the near-critical gas-plasma at $t = 56T$ is shown in Fig.2(a). For clarity, only a part of the simulation box is shown. The spot size of the laser is focused to be smallest at $z = 35\mu m$, and the transverse electric field is enhanced to 17 there, which is 1.7 times higher than the initial laser electric field. The pulse retains

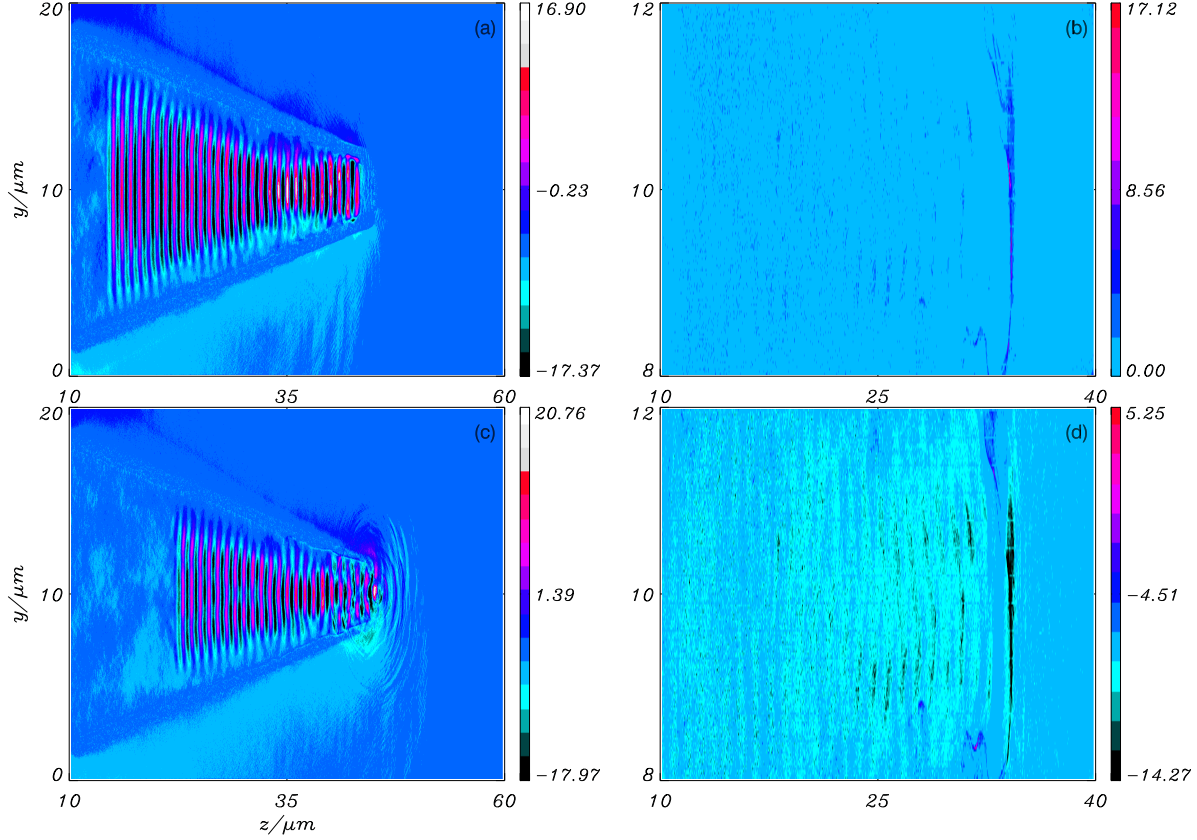


FIG. 2: (color online). Left: Transverse electric field (in units of $m_e c \omega / e$) at (a) $t = 56T$, (c) $t = 64T$. Right: (b) electron density (in units of critical density n_c), and (d) the longitudinal electron current J_{ze} (in units of $en_c c$) at $t = 44T$.

its Gaussian radial profile, however, its spot size varies with the distance of propagation in a periodic manner. The smallest spot size at $z = 35\mu m$ is about $3\mu m$, while it varies to about $4\mu m$ at $z = 40\mu m$. This result is due to dynamic balance between diffraction and non-linear self-focusing, which is also in good agreement with the analysis of the paraxial ray approximation[41]. When the laser propagates to the tip of the cone, it is even focused or squeezed by the tip of the cone for the small radius there, as is shown in Fig.2(b). The spot size is focused to about $1\mu m$ at the tip of the cone($z = 45\mu m$), with the transverse electric field as high as 20 there. The electrons that are initially at the front of the pulse are more efficiently accelerated as the pulse undergoes intensity enhancement due to self-focusing. Strong flows of relativistic electrons, axially comoving with the laser pulse, are observed

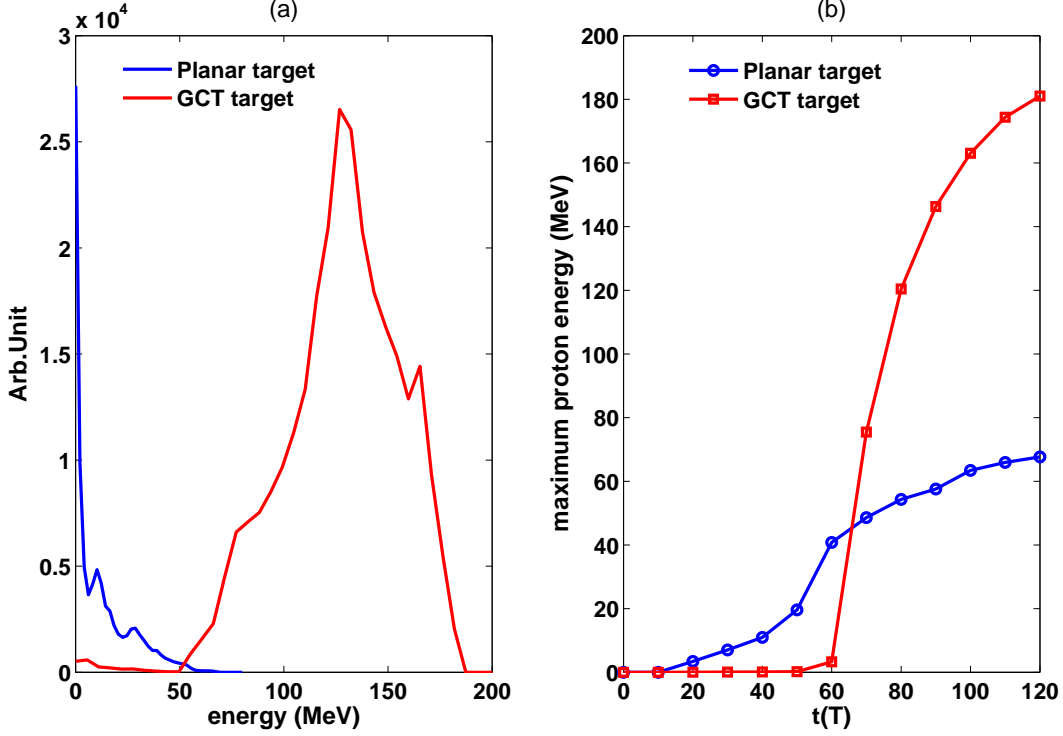


FIG. 3: (color online). (a) the proton energy spectrum of the protons behind the targets for different cases at $t=120T$. and (b) Evolution of the maximum proton energy for different cases.

in the simulation, as shown in Fig.2(b) and Fig.2(d). The maximum electron density near the axis is as high as $17n_c$, and the longitudinal electron current $J_{ze} = -en_e v_{ze}$ is about $-14en_c c$ (negative J_{ze} due to negative electron charge). These energetic electrons then transport through the thin foil and form a strong backside sheath field there.

Fig.3(a) shows the energy spectrum of the proton bunches behind the targets in the two cases at $t = 120T$. For the case shown, the maximum energy for the GCT target is about 181 MeV, which is nearly three times higher than that of the planar target (65 MeV) under the same conditions. The energy conversion efficiencies from laser to protons are 2.5% and 0.7% for GCT and planar targets at $t = 120T$, respectively. For the GCT target, due to the small transverse size of the foil where the sheath field is homogenous, the energy spectrum of the proton bunch has a quasi-monoenergetic peak with energy dispersion of about 36%. In contrast, the energy spectrum from the planar target is much broadened due to multidimensional effects such as hole boring and other instabilities. The evolution of the maximum proton energy is shown in Fig.3(b). For the planar target, as the laser impinges

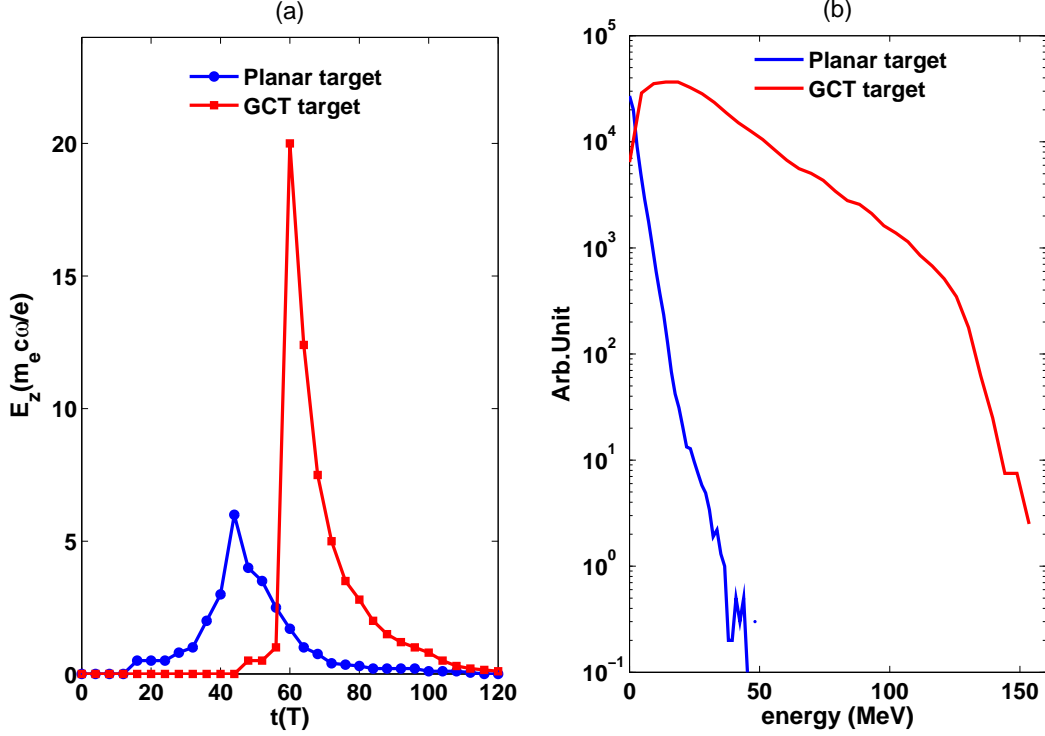


FIG. 4: (color online). (a) Evolution of the electrostatic fields at the place of the proton layer for the two cases of planar and GCT target and (b) the electron energy spectrum of the protons behind the targets at $t=50T$ for planar target and $t=80T$ for GCT target.

on the target at $t = 10T$ (the planar target is initially located at $z = 10\mu m$), the maximum proton energy increases earlier than the GCT target (for which the laser impinges on the foil at $t = 60T$). However, as the electrostatic field at the place of the proton layer is much weaker for the planar target (see in Fig.4(a)), the increase of proton energy is much slower than the GCT target. For the GCT target, the maximum proton energy increases rapidly from 3.3MeV to 120MeV in only 20T (from $t = 60T$ to $t = 80T$), which is attributed to the strong electrostatic field during that time. At later time, the maximum proton energies in both cases remain almost constant.

Evolutions of the electrostatic fields at the place of the proton layer for the planar and GCT targets are shown in Fig.4(a), which explains the energy enhancement of GCT target in Fig.3(b). The electrostatic fields straight up quickly at $t = 60T$ for the GCT target when the laser impinges on the target, because the energetic electrons generated from the gas-plasma reach the back side of the foil at $t = 60T$ and establish a strong sheath field there (see

in Fig.5(a)). The maximum electrostatic field is about 20 for GCT target at $t = 60T$, which is about 3.3 times higher than the planar target(6 at $t = 44T$). Since the energetic electrons expand away quickly, the electric fields decrease quickly after reaching the maximum for both cases. The electron energy spectrums behind the targets at $t=50T$ for planar target and $t=80T$ for GCT target are shown in Fig.4(b), at both times when the maximum energy of the electrons behind the targets is highest. We can see that the electron temperature and density are higher for the GCT target, which will result in a higher longitudinal field and eventually higher proton energy, as shown in Fig.4(a) and Fig.3(a).

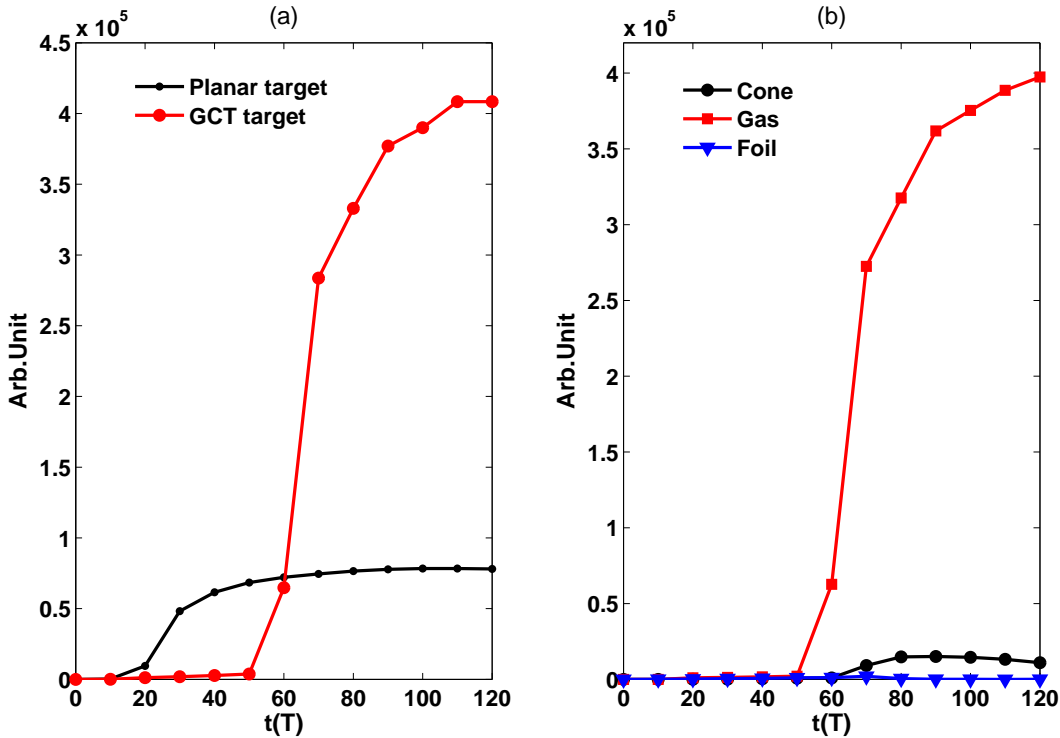


FIG. 5: (color online).(a) Time evolution of the number of electrons behind the planar and GCT targets. (b)Time evolution of the number of electrons behind the planar originated from different places.

Since the TNSA mechanism depends strongly on the charge separation field established by the energetic electrons, it is of interest to investigate the electron number behind the target. Fig.5(a) shows the time evolution of electron number behind the planar and GCT targets. For both cases, the electron numbers initially increase after the laser irradiates on the targets, and then flatten out. For GCT target, the electron number is nearly 5 times

higher than the planar target at $t = 120T$. From Fig.5(b) we can see the energetic electrons are almost generated from the gas-plasma (97% of the total number), while only a small number of the electrons are from the cone (3% of the total number). This result indicates that with the GCT target the efficiency of proton acceleration is determined by the electrons generated from the gas, which is quite different from the planar target(the electrons are from the target itself).

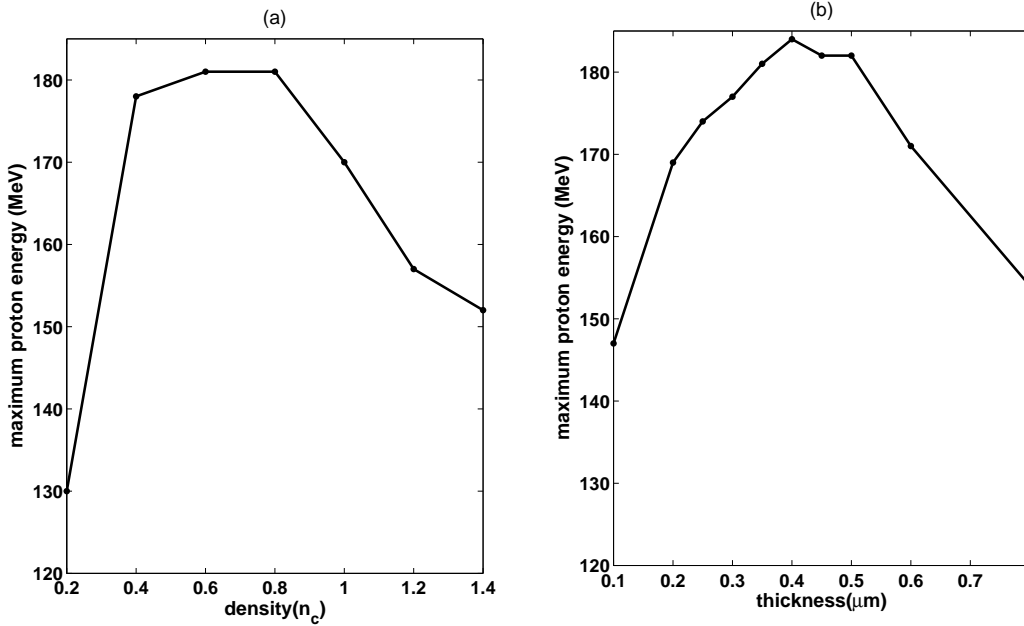


FIG. 6: (color online).(a) Maximum proton energy for different gas-plasma density. (b) Maximum proton energy for different foil thickness.

The effects of the gas-plasma density and the foil thickness of the GCT target are shown in Fig.6. It is found that the maximum proton energy remains almost the same(near 180MeV) while the gas-plasma density is between $0.4n_c$ and $0.8n_c$, and the foil thickness is between $0.3\mu m$ and $0.5\mu m$. These simulation results demonstrate that our acceleration scheme is robust. On the other hand, for the gas-plasma density, over-high gas-plasma density will result in much depletion of laser pulse, while over-low gas-plasma density will leads fewer energetic electrons behind the foil, both will result in a decrease of the maximum proton energy. For the foil thickness, thin foils proved to be more efficient for ion acceleration in TNSA by hot-Electron recirculation[42], but over-thin foil will result in a quick expanding of the electrons, which will also result in a lower proton energy.

We have also stimulated the interaction of a Linear polarized(LP) laser pulse with a GCT target at the same intensity, while the other parameters are the same as in Fig.1. Our simulations results verify that similar phenomenon can also be observed with the LP laser pulse. A quasi-monoenergetic proton beam with peak energy of 139 MeV and maximum energy of 185 MeV can be generated. This indicates that our acceleration scheme can be also efficient for the LP laser pulse.

IV. CONCLUSION

In conclusion, proton acceleration from a GCT target is proposed to enhance the ion energy. A quasi-monoenergetic proton bunch with peak energy of 130MeV and maximum energy of 181MeV is achieved by using the GCT target at laser intensity of $2.6 \times 10^{20} W/cm^2$. It is nearly three times higher than that from the planar target. This result is attributed to a stronger electrostatic field behind the foil, which is formed by the energetic electrons generated and accelerated by the enhanced laser pulse in the gas-plasma. The effects of the gas-plasma density and the foil thickness have been investigated. The results demonstrate that our acceleration scheme is robust. Such GCT target may be difficult to make at present, however, with the rapid advance in nanofabrication technology such a small conical channel filled with gas-plasma should be realizable[43]. Accordingly, the GCT target can remarkably reduce the cost of a laser driven ion accelerator in the applications such as cancer therapy.

Acknowledgments

This work was supported by National Nature Science Foundation of China (Grant Nos. 10935002,10835003,11025523) and National Basic Research Program of China (Grant No. 2011CB808104). XQY would like to thank the support from the Alexander von Humboldt Foundation.

-
- [1] M. Borghesi, D. H. Campbell, A. Schiavi, M. G. Haines, O. Willi, A. J. MacKinnon, P. Patel, L. A. Gizzi, M. Galimberti, R. J. Clarke, F. Pegoraro, H. Ruhl, and S. Bulanov , *Phys. Plasmas* **9**, 2214 (2002).

- [2] N. Naumova, T. Schlegel, V. T. Tikhonchuk, C. Labaune, I. V. Sokolov, and G. Mourou, *Phys. Rev. Lett* **102**, 025002 (2009).
- [3] M. Roth, T. E. Cowan, M. H. Key, S. P. Hatchett, C. Brown, W. Fountain, J. Johnson, D. M. Pennington, R. A. Snavely, S. C. Wilks, K. Yasuike, H. Ruhl, F. Pegoraro, S. V. Bulanov, E. M. Campbell, M. D. Perry, and H. Powell, *Phys. Rev. Lett* **86**, 436 (2001).
- [4] M. Temporal, J. J. Honrubia, and S. Atzeni, *Phys. Plasmas* **9**, 3098 (2002).
- [5] S. V. Bulanov and V. S. Khoroshkov, *Plasma Phys. Rep* **28**, 453 (2002).
- [6] J. Denavit, *Phys. Rev. Lett* **69**, 3052 (1992).
- [7] L. O. Silva, M. Marti, J. R. Davies, R. A. Fonseca, C. Ren, F. Tsung, and W. B. Mori, *Phys. Rev. Lett* **92**, 015002 (2004).
- [8] X. Q. Yan, C. Lin, Z. M. Sheng, Z. Y. Guo, B. C. Liu, Y. R. Lu, J. X. Fang, and J. E. Chen, *Phys. Rev. Lett* **100**, 135003 (2008).
- [9] Z. M. Sheng, K. Mima, Y. Sentoku, K. Nishihara, and J. Zhang , *Phys. Plasmas* **9**, 3147 (2002).
- [10] A. Henig, D. Kiefer, K. Markey, D. C. Gautier, K. A. Flippo, S. Letzring, R. P. Johnson, T. Shimada, L. Yin, B. J. Albright, K. J. Bowers, J. C. Fernández, S. G. Rykovanov, H.-C. Wu, M. Zepf, D. Jung, V. Kh. Liechtenstein, J. Schreiber, D. Habs, and B. M. Hegelich, *Phys. Rev. Lett* **103**, 045002 (2009).
- [11] B. Qiao, M. Zepf, M. Borghesi, and M. Geissler, *Phys. Rev. Lett* **102**, 145002 (2009).
- [12] X. Q. Yan, H. C. Wu, Z. M. Sheng, J. E. Chen, and J. Meyer-ter-Vehn, *Phys. Rev. Lett* **103**, 135001 (2009).
- [13] E. Fourkal, I. Velchev, and C. M. Ma, *Phys. Rev. E* **71**, 036412 (2005).
- [14] J. Fuchs, P. Antici, E. D’Humieres, E. Lefebvre, M. Borghesi, E. Brambrink, C. A. Cecchetti, M. Kaluza, V. Malka, M. Manclossi, S. Meyroneinc, P. Mora, J. Schreiber, T. Toncian, H. Pépin, and P. Audebert, *Nat. Phys* **2**, 48 (2006).
- [15] S. C. Wilks, A. B. Langdon, T. E. Cowan, M. Roth, M. Singh, S. Hatchett, M. H. Key, D. Pennington, A. MacKinnon, and R. A. Snavely, *Phys. Plasmas* **8**, 542 (2001).
- [16] R. A. Snavely, M. H. Key, S. P. Hatchett, T. E. Cowan, M. Roth, T. W. Phillips, M. A. Stoyer, E. A. Henry, T. C. Sangster, M. S. Singh, S. C. Wilks, A. MacKinnon, A. Offenberger, D. M. Pennington, K. Yasuike, A. B. Langdon, B. F. Lasinski, J. Johnson, M. D. Perry, and E. M. Campbell, *Phys. Rev. Lett* **85**, 2945 (2000).

- [17] H. Schwoerer, S. Pfotenhauer, O. Jäckel, K.-U. Amthor, B. Liesfeld, W. Ziegler, R. Sauerbrey, K. W. D. Ledingham, and T. Esirkepov, *Nature* **439**, 445 (2006).
- [18] B. M. Hegelich, B. J. Albright, J. Cobble, K. Flippo, S. Letzring, M. Paffett, H. Ruhl, J. Schreiber, R. K. Schulze, and J. C. Fernández, *Nature* **439**, 441 (2006).
- [19] R. Kodama, P. A. Norreys, K. Mima, A. E. Dangor, R. G. Evans, H. Fujita, Y. Kitagawa, K. Krushelnick, T. Miyakoshi, N. Miyanaga, T. Norimatsu, S. J. Rose, T. Shozaki, K. Shigemori, A. Sunahara, M. Tampo, K. A. Tanaka, Y. Toyama, T. Yamanaka, and M. Zepf, *Nature (London)* **412**, 798 (2001).
- [20] Z. L. Chen, R. Kodama, M. Nakatsutsumi, H. Nakamura, M. Tampo, K. A. Tanaka, Y. Toyama, T. Tsutsumi, and T. Yabuuchi, *Phys. Rev. E* **71**, 036403 (2005).
- [21] R. B. Stephens, S. P. Hatchett, R. E. Turner, K. A. Tanaka, and R. Kodama, *Phys. Rev. Lett* **91**, 185001 (2003).
- [22] L. V. Woerkom, K. U. Akli, T. Bartal, F. N. Beg, S. Chawla, C. D. Chen, E. Chowdhury, R. R. Freeman, D. Hey, M. H. Key, J. A. King, A. Link, T. Ma, A. J. MacKinnon, A. G. MacPhee, D. Offermann, V. Ovchinnikov, P. K. Patel, D. W. Schumacher, R. B. Stephens, and Y. Y. Tsui, *Phys. Plasmas* **15**, 056304 (2008).
- [23] R. J. Mason, *Phys. Rev. Lett* **96**, 035001 (2006).
- [24] A. L. Lei, K. A. Tanaka, R. Kodama, G. R. Kumar, K. Nagai, T. Norimatsu, T. Yabuuchi, and K. Mima, *Phys. Rev. Lett* **96**, 255006 (2006).
- [25] J. Pasley, and R. Stephens, *Phys. Plasmas* **14**, 054501 (2007).
- [26] H. Sakagami, T. Johzaki, H. Nagatomo, and K. Mima, *Laser Part. Beams* **24**, 191 (2006).
- [27] H. Nagatomo, T. Johzaki, T. Nakamura, H. Sakagami, A. Sunahara, and K. Mima, *Phys. Plasmas* **14**, 056303 (2007).
- [28] M. H. Key, *Phys. Plasmas* **14**, 055502 (2007).
- [29] H. B. Cai, K. Mima, W. M. Zhou, T. Jozaki, H. Nagatomo, A. Sunahara, and R. J. Mason, *Phys. Rev. Lett* **102**, 245001 (2009).
- [30] J. A. King, K. U. Akli, R. R. Freeman, J. Green, S. P. Hatchett, D. Hey, P. Jamangi, M. H. Key, J. Koch, K. L. Lancaster, T. Ma, A. J. MacKinnon, A. MacPhee, P. A. Norreys, P. K. Patel, T. Phillips, R. B. Stephens, W. Theobald, R. P. J. Town, L. Van Woerkom, B. Zhang, and F. N. Beg, *Phys. Plasmas* **16**, 020701 (2009).
- [31] J. S. Green, K. L. Lancaster, K. U. Akli, C. D. Gregory, F. N. Beg, S. N. Chen, D. Clark,

- R. R. Freeman, S. Hawkes, C. Hernandez-Gomez, H. Habara, R. Heathcote, D. S. Hey, K. Highbarger, M. H. Key, R. Kodama, K. Krushelnick, I. Musgrave, H. Nakamura, M. Nakatsutsumi, N. Patel, R. Stephens, M. Storm, M. Tampo, W. Theobald, L. Van Woerkom, R. L. Weber, M. S. Mei, N. C. Woolsey, and P. A. Norreys, *Nat. Phys* **3**, 853 (2007).
- [32] J. Rassuchine, E. dHumières, S. D. Baton, P. Guillou, M. Koenig, M. Chahid, F. Perez, J. Fuchs, P. Audebert, R. Kodama, M. Nakatsutsumi, N. Ozaki, D. Batani, A. Morace, R. Redaelli, L. Gremillet, C. Rousseaux, F. Dorchie, C. Fourment, J. J. Santos, J. Adams, G. Korgan, S. Malekos, S. B. Hansen, R. Shepherd, K. Flippo, S. Gaillard, Y. Sentoku, and T. E. Cowan, *Phys. Rev. E* **79**, 036408 (2009).
- [33] Y. Sentoku, K. Mima, H. Ruhl, Y. Toyama, R. Kodama, and T. E. Cowan, *Phys. Plasmas* **11**, 3083 (2004).
- [34] T. Nakamura, T. Nakamura, H. Sakagami, T. Johzaki, H. Nagatomo, K. Mima, and J. Koga, *Phys. Plasmas* **14**, 103105 (2007).
- [35] L. H. Cao, W. Yu, M. Y. Yu, H. Xu, X. T. He, Y. Q. Gu, Z. J. Liu, J. H. Li, and C. Y. Zheng, *Phys. Rev. E* **78**, 036405 (2008).
- [36] A. Pukhov, and J. Meyer-ter-Vehn, *Phys. Rev. Lett* **76**, 21 (1996).
- [37] W. B. Mori, C. Joshi, J. M. Dawson, D. W. Forslund, and J. M. Kindel, *Phys. Rev. Lett* **60**, 1298 (1988).
- [38] W. B. Mori, *IEEE J. Quant. Electron* **33**, 1942 (1997).
- [39] M. V. Asthana, A. Giulietti, D. Giulietti, L. A. Gizzi, and M. S. Sodha, *Laser Part. Beams* **18**, 399 (2000).
- [40] D. Tripathi, L. Bhasin, R. Uma, and V. K. Tripathi, *Phys. Plasmas* **17**, 113113 (2010).
- [41] A. Panwar, and A. K. sharma, *Laser Part. Beams* **27**, 249 (2009).
- [42] A. J. Mackinnon, Y. Sentoku, P. K. Patel, D. W. Price, S. Hatchett, M. H. Key, C. Andersen, R. Snavely, and R. R. Freeman, *Phys. Rev. Lett* **88**, 215006 (2002).
- [43] K. Ostrikov, *Rev. Mod. Phys* **77**, 489 (2005).